Protein Engineering, Design & Selection vol. 22 no. 3 pp. 135–147, 2009
Published online February 1, 2009 doi:10.1093/protein/gzn079

Stabilization and humanization of a single-chain Fv antibody fragment specific for human lymphocyte antigen CD19 by designed point mutations and CDR-grafting onto a human framework

Markus Kügler[1], Christoph Stein[1], Michael Schwenkert[1], Domenica Saul[1], Lena Vockentanz[1,3], Thomas Huber[2,4], Svava K. Wetzel[2], Oliver Scholz[2], Andreas Plückthun[2], Annemarie Honegger[2,5] and Georg H. Fey[1]

[1]Chair of Genetics, Institute of Biology, University of Erlangen-Nuremberg, Erwin-Rommel-Strasse 3, D-91058 Erlangen, Germany, [2]Biochemisches Institut der Universität Zürich, Winterthurerstrasse 190, CH-8057 Zürich, Switzerland, [3]Present address: Max-Delbrück-Centrum für Molekulare Medizin, Robert-Rössle-Straße 10, D-13125 Berlin-Buch, Germany and [4]Present address: Novartis Biologics/Protein Design, WSJ-506.3.13, Novartis Pharma AG, CH-4002 Basel, Switzerland.

[5]To whom correspondence should be addressed.
E-mail: honegger@bioc.uzh.ch

A single-chain Fv (scFv) fragment derived from the murine antibody 4G7, specific for human lymphocyte CD19, was engineered for stability and expression in *Escherichia coli* in view of future use as a therapeutic protein. We compared two orthogonal knowledge-based procedures. In one approach, we designed a mutant with 14 single amino-acid substitutions predicted to correct destabilizing residues in the 4G7-wt sequence to create 4G7-mut. In the second variant, the murine CDRs were grafted to the human acceptor framework huVκ3-huV$_H$3, with 11 additional point mutations introduced to obtain a better match between CDR graft and acceptor framework, to arrive at 4G7-graft. Compared to 4G7-wt, 4G7-mut showed greater thermodynamic stability in guanidinium chloride-induced equilibrium denaturation experiments and somewhat greater stability in human serum. The loop graft maintained the comparatively high stability of the murine loop donor, but did not improve it further. Our analysis indicates that this is due to subtle strain introduced between CDRs and framework, mitigating the otherwise highly favorable properties of the human acceptor framework. This slight strain in the loop graft is also reflected in the binding affinities for CD19 on leukemic cells of 8.4 nM for 4G7-wt, 16.4 nM for 4G7-mut and 30.0 nM for 4G7-graft. This comparison of knowledge-based mutation and loop-grafting-based approaches will be important, when moving molecules forward to therapeutic applications.

Keywords: antibody engineering/CDR graft/immunoglobulin variable domains/scFv fragment/stability

Introduction

The surface antigen CD19, a 95 kDa transmembrane glycoprotein of the immunoglobulin superfamily, is selectively expressed on mammalian B-lymphoid cells in most stages of differentiation from the early pro-B-cell stage on, but not on plasma cells and hematopoietic stem cells. Together with CD21, CD81 and Leu13 (CD225), CD19 forms the B-cell receptor co-complex and plays a role in the control of differentiation, activation and proliferation of B-lymphoid cells (Sato *et al*., 1997). The antigen is present on the blasts of different types of human B-cell malignancies including pro- and pre-B-cell acute lymphoblastic leukemias (ALL), common ALL (cALL) of children and young adults, non-Hodgkin-lymphomas (NHL), chronic B-lymphocytic leukemia (B-CLL) and hairy-cell leukemia (HCL) (Nadler *et al*., 1983). It is not shed from malignant cells and is internalized after binding of antibodies and single-chain Fv (scFv) antibody fragments (Press *et al*., 1989). Antigen density ranges from 10 000 to 30 000 molecules per cell on healthy peripheral B-cells, and from 7000 to 30 000 molecules per cell on malignant cells from a variety of lymphoid cancers (Olejniczak *et al*., 2006). Due to these properties, CD19 is an attractive target for the design of antibody-based therapeutics for the treatment of B-cell neoplasias (Grossbard *et al*., 1992). In addition, agents targeting CD19 may also become useful for the treatment of chronic inflammatory diseases and some autoimmune disorders.

A number of antibody derivatives targeting CD19 have been tested for the treatment of B-cell cancers, so far with modest success. Unconjugated CD19 antibodies produced promising results in pre-clinical tests, but no therapeutic benefit in clinical trials (Hekman *et al*., 1991; Pietersz *et al*., 1995; Lang *et al*., 2004; Yazawa *et al*., 2005). Immunotoxins consisting of plant or bacterial toxins coupled either to whole antibodies or fused to scFv fragments specific for a number of surface antigens of B-lymphoid cells were designed (Pastan *et al*., 2007). Ricin derivatives coupled to whole IgGs specific for CD19 were extensively tested, but have not progressed beyond phase II clinical studies due to serious side effects (Messmann *et al*., 2000; Schindler *et al*., 2001). Recombinant immunotoxins consisting of CD19-specific scFv-fragments coupled to saporin and diphtheria toxin are under current investigation (Vallera *et al*., 2005; Flavell *et al*., 2006), but have not been advanced to clinical testing. A fusion protein between an anti-CD19 scFv and a fragment of *Pseudomonas* Exotoxin A was effective in pre-clinical tests (Schwemmlein *et al*., 2007), and investigators have conjugated potent novel small-molecule toxins such as duocarmycins and maytansinoids (Erickson *et al*., 2006; Chari, 2008) to anti-CD19 antibodies. Finally, CD19-specific scFv fragments have been coupled to death-effectors such as FAS- and TRAIL-ligands, and a CD19 scFv fused to a soluble TRAIL-ligand (sTRAIL) had attractive pre-clinical activities on human malignant cells (Stieglmaier *et al*., 2008).

A number of different bispecific formats targeting CD19 in combination with different specificities were examined as

well. Full-length antibodies and Fab-fragments targeting CD19 were effective in pre-clinical studies, but not in clinical trials (Peipp and Valerius, 2002). Recombinant bispecific scFv-derivatives targeting CD19 have also been tested for recruiting Natural Killer (NK) cells as effectors for tumor cell lysis by binding to the low affinity FcγRIIIa receptor (CD16) on NK-cells, monocytes and macrophages (Kipriyanov *et al*., 2002; Bruenke *et al*., 2005). This has been achieved either in a diabody format (Kipriyanov *et al*., 2002) or by tandemly arranged scFv fragments, each encoding an interchain disulfide bond (Bruenke *et al*., 2005). A variant of this format are tandem diabodies ('tandabs'), non-covalently associated two-chain molecules, which form two scFv binding sites each for the tumor antigen and the trigger molecule on the effector cell. Such a molecule specific for CD19 and CD3 was effective in pre-clinical tests (Bruenke *et al*., 2005). Another recently developed variant format carries two distal CD19-specific scFvs plus a central CD16-specific scFv in a tandem linear arrangement (Kellner *et al*., 2008) (termed triplebody). In pre-clinical studies, this molecule produced potent ADCC (antibody dependent cellular cytotoxicity) reactions with human leukemic cells as targets and enriched human NK-cells as effectors, and the format is therefore attractive for further development towards clinical testing. The bispecific molecule targeting CD19 that currently has advanced furthest is Blinatumomab, a tandem scFv carrying specificities for CD19 and CD3, a cofactor of the T-cell receptor on human T lymphocytes. The anti-CD3 specificity recruits and activates T-cells for tumor cell lysis, regardless of the antigen-specificity of their T-cell receptors, and the T-cells have high cytotoxic potential. The molecule produced objective responses in a phase I clinical trial with non-Hodgkin lymphoma patients and is promising for clinical development (Bargou *et al*., 2008). Nevertheless, for some applications, such as the treatment of pediatric ALL patients in a post-transplantation stage, T-cells may not be present in sufficient numbers to serve as an efficient effector cell population. Therefore, a need remains to develop CD19-specific agents in other formats, such as immunotoxins, immunoconjugates with other types of death-effectors and bispecific molecules recruiting effectors other than T-cells. Moreover, all of the above formats will profit from well designed, stable scFv derivatives with human sequences, in order to avoid production problems for clinical trials, and loss of activity after prolonged incubation in human serum due to denaturation and aggregation. It should be pointed out that many of the above molecules could not even be produced in *Escherichia coli*, but the investigators had to resort to production in mammalian cells, suggesting an aggregation propensity of the molecules.

For therapeutic applications in humans, CD19-specific scFv antibody fragments need to have high thermodynamic stability and should be humanized to avoid a neutralizing antibody response (Mirick *et al*., 2004). The antigenicity problem is less severe for agents used to treat B-cell neoplasias, because these patients have an impaired B-cell compartment and produce fewer neutralizing antibodies, allowing the use of bacterial toxins (Pastan *et al*., 2007). However, some patients may require CD19-specific agents for extended periods of time. While human antibodies can be derived from genetically modified mice carrying immunoglobulin loci (Lonberg, 2005) or by screening synthetic phage display libraries carrying natural or designed human antibody fragments (Knappik *et al*., 2000; Hoogenboom, 2005), in this study, we wished to start from a well characterized murine hybridoma, termed 4G7 (Meeker *et al*., 1984).

The scFv derived from the antibody 4G7 had already shown favorable biological activities in bispecific scFv constructs (Bruenke *et al*., 2005). We analyzed its biophysical properties in the present study and found them to be already rather favorable. Nonetheless, to test whether the molecule can be improved further in its biophysical properties, we took two orthogonal approaches. We first analyzed the murine scFv for sequence features associated with poor folding and low stability and designed a series of 14 point mutations addressing two major and multiple minor problems, while preserving the structural characteristics of the original antibody variable domains. In parallel, we designed a CDR graft to a human framework. We used the most stable of the human germline family consensus frameworks, huVκ3-huV$_H$3, despite the fact that the murine and human V$_L$ sequence showed only 53% sequence identity, and the two V$_H$ domains shared a mere 51% sequence identity. Additionally, in this graft, we had a mismatch between the structural subtypes (Honegger *et al*., 2009) of V$_H$ CDR donor and acceptor framework, which may be responsible for the fact that such grafts frequently fail to reach the degree of stabilization expected from the superior properties of the acceptor framework (Willuda *et al*., 1999). In the companion paper, we have directly addressed the antibody engineering problems caused by such a mismatch in a series of chimeric V$_H$ constructs (Honegger *et al*., 2009). In the present paper, we compare the stabilization that can be achieved with a limited number of point mutations introduced into the original framework to the stability achieved by grafting to a mismatched framework of otherwise proven stability, and compare both of these proteins to the 4G7-wt.

Materials and methods

Homology modeling of the 4G7 Fv fragment

A homology model of the 4G7 Fv fragment was built based on the structures of the V$_L$ domain of the esterolytic murine antibody Fab fragment MS6-12 [PDB entry 1MJU (Ruzheinikov *et al*., 2003)] and the V$_H$ domain structures of an anti-ssDNA Fab fragment [1P7K (Schuermann *et al*., 2004)], anti-rhodopsin Fab fragment K42-41L [1XGY (Piscitelli *et al*., 2006)] and the Fab fragment of bactericidal antibody MN12H2 [1MNU (van den Elsen *et al*., 1999)]. Modeling of the huVκ3-huV$_H$3 germline consensus Fv has been reported previously (Knappik *et al*., 2000). The two models were combined to produce the model of the CDR graft construct 4G7-graft in a relative domain orientation intermediate between those observed in the two antibody fragments serving as primary template for the V$_L$ and the V$_H$ domain.

Culture of eukaryotic cells

Leukemia-derived SEM (t(4;11)-positive pro-B-ALL; (Greil *et al*., 1994)) and CEM cells (T-ALL; DSMZ, German Collection of Microorganisms and Cell Lines, Braunschweig, Germany) were cultured in RPMI 1640-Glutamax-I medium (Invitrogen, Karlsruhe, Germany), supplemented with 10% fetal calf serum and penicillin and streptomycin (Invitrogen) at concentrations of 100 U/ml and 100 μg/ml, respectively.

Bacterial strains and plasmids

Escherichia coli XL1-Blue (Stratagene, Amsterdam, The Netherlands) was used for the amplification of plasmids and cloning. The expression vector pAK400 (Krebber *et al*., 1997) was used for the expression of antibody fragments in *E.coli* HB2151 (Carter *et al*., 1985) (from Dr G. Winter, MRC Cambridge, UK) and the vector pASK4 (IBA, Göttingen, Germany) was used as an intermediate cloning vector for the construction of the mutant 4G7-mut.

Construction of expression vectors

The sequence coding for the murine anti-CD19-4G7 wild-type scFv (4G7-wt) was excised as an SfiI cassette from a previously cloned pAK100 vector construct (Krebber *et al*., 1997; Peipp *et al*., 2004). It is of the format V_L-$(Gly_4Ser)_4$-V_H. The cassette was inserted by directional cloning into the prokaryotic expression vector pAK400, which provides an N-terminal FLAG-tag and a C-terminal His_6-tag. For construction of the mutant 4G7-mut, the SfiI cassette was transferred from 4G7-wt into the intermediate vector pASK4. The 14 amino acid substitutions were introduced by PCR reactions (site-directed mutagenesis) and oligonucleotide annealing using the QuickChange® Multi SiteDirected Mutagenesis Kit (Stratagene, La Jolla, CA, USA) according to the manufacturer's instructions. For the oligonucleotide annealing experiments, complementary primers were designed containing the desired mutations and specific restriction site overlaps. After annealing by heating a primer mixture to 96°C and subsequent cooling to 25°C for 30 min, these overlaps were used to ligate the complementary primers into a correspondingly digested vector. Correct incorporation of the desired mutations was checked by DNA sequencing before the sequence coding for 4G7-mut was re-cloned into the expression vector pAK400.

The gene for the loopgrafted 4G7 scFv variant (huV_H3-4G7-graft), including codon optimization for the production in *E.coli*, was synthesized by Entelechon (Regensburg, Germany). An SfiI cassette containing the huV_H3-4G7-graft coding sequence was then excised from the commercial standard vector and subcloned into the expression vector pAK400.

Soluble periplasmic expression

For soluble expression of the 4G7 scFvs, expression plasmids were propagated in *E.coli* HB2151. Overnight cultures were incubated at 37°C and diluted in Tryptone Broth medium [TB; 12 g/l bacto-tryptone, 24 g/l bacto-yeast extract, 4 ml/l glycerol, 100 ml/l 10× TB phosphate (0.17 M KH_2PO_4, 0.72 M K_2HPO_4)] supplemented with 1% glucose and 30 μg/ml chloramphenicol until an extinction of 0.2 at 600 nm (OD_{600}) was reached. Cultures were incubated at 28°C and expression was induced at an OD_{600} of 0.8 by addition of isopropyl-β-D-thiogalactopyranoside (IPTG) to a final concentration of 1 mM. After 18 h of incubation, cells were collected by centrifugation, resuspended in 1/10 volume of homogenization buffer containing 50 mM NaH_2PO_4, pH 8.0, 300 mM NaCl and 10 mM imidazole. After disruption of cells by high-pressure in an EmulsiFlex-C5 homogenizer (Avestin, Canada), the crude extract was centrifuged to remove debris (28 000*g*, 60 min at 4°C) and the supernatant was used for a two-step purification.

Two-step purification of scFvs

Purification of His_6-tagged scFv fragments was achieved by affinity chromatography with a nickel-nitrilotriacetic acid (Ni-NTA, Qiagen) matrix. For this purpose, 400 μl NiNTA slurry was added per 100 ml of supernatant, and the mixture was incubated for 30 min at 25°C. The suspension was transferred to an empty column (BioRad) and the matrix was washed extensively with MHA high-salt wash buffer [20 mM MHA (6.6 mM MES, 6.6 mM HEPES, 6.6 mM sodium acetate), pH 7.0, 1 M NaCl], then with MHA low-salt wash buffer (20 mM MHA, pH 7.0, 100 mM NaCl) and finally with MHA imidazole wash buffer (20 mM MHA, pH 7.0, 30 mM imidazole) to remove unspecifically bound proteins. The His-tagged antibody fragments were then eluted by adding 250 mM imidazole. The eluate was extensively dialyzed against 20 mM MHA, containing 60 mM imidazole, and was applied to a HiTrap SP XL column (GE Healthcare, Freiburg, Germany) for ion exchange chromatography. Loading was performed in 20 mM MHA (pH 7.0, 60 mM imidazole) using an ÄKTA Prime chromatography system (Amersham Pharmacia Biotech, Freiburg, Germany). A NaCl gradient from 0 to 500 mM was used to elute the scFvs from the column. Collected fractions were checked for the presence of scFvs by SDS–PAGE analysis and pooled fractions were extensively dialyzed against 50 mM Tris–HCl (pH 7.2). The purity of the antibody fragments was checked by SDS–PAGE analysis and the concentration was determined by measuring the absorbance at 280 nm. The second purification step removed the 22 kDa SlyD, which carries a natural his-rich sequence (Wülfing *et al*., 1994).

Measurement of expression yields

To determine expression yields of the 4G7 scFvs, aliquots of the Ni-NTA (Qiagen) purified and dialyzed proteins were analyzed by SDS–PAGE. The purity was assessed and the concentration was estimated by densitometric comparison to bovine serum albumin standards. Expression yields were calculated as mg of purified scFv per liter of *E.coli* culture and microgram of purified scFv per gram of *E.coli* pellet.

SDS–PAGE and western blot analysis

SDS–PAGE was carried out under reducing conditions following standard procedures. Gels were stained with Coomassie Brilliant Blue R250. For western-blot analysis, scFv fragments were detected with a Penta-His antibody (Qiagen) and a secondary goat anti-mouse IgG antibody coupled to horseradish peroxidase (Dianova, Hamburg, Germany). Blots were developed with the enhanced chemiluminescence reagent (Amersham Pharmacia Biotech, Freiburg, Germany).

Analytical Gel-filtration chromatography

For the determination of the aggregation tendency of purified scFvs, samples were analyzed by size exclusion chromatography on a Superdex75 column 10/300GL (GE Healthcare) equilibrated with 50 mM sodium phosphate (pH 7.0) and 100 mM NaCl on an Agilent 1100 HPLC system (Agilent). Samples were injected at a concentration of 0.5 mg/ml (17 μM) in a volume of 50 μl, the flow rate was 0.5 ml/min and elution was followed by the detection of the absorbance at 280 nm. A mini-DAWN multi-angle light scattering

(MALS) detector (Wyatt Technology) and a differential refractometer (Optilab rEX, Wyatt Technology) were used for the determination of the absolute molar mass of the scFv variants. The concentration was calculated assuming a dn/dc of 0.185.

Flow cytometric analysis and competition binding studies

Binding of scFvs to CD19 positive SEM cells was analyzed on a FACS Calibur instrument using CellQuest software (Becton Dickinson, Heidelberg, Germany) following published procedures (Bruenke *et al*., 2004). Ten thousand events were collected for each sample and all analyses of whole cells were performed using appropriate scatter gates to exclude cellular debris and aggregates. The scFvs were detected using an Anti-Penta-His antibody and a phycoerythrin (PE)-conjugated goat anti-mouse IgG antibody (DAKO Diagnostica, Hamburg, Germany). For competition binding experiments, cells were pre-incubated with a 50-fold molar excess of either the parental monoclonal antibody 4G7 or a mouse IgG1 isotype control antibody for 15 min before addition of the scFvs.

Determination of equilibrium dissociation constants (K_D) by flow cytometry

Equilibrium dissociation constants (K_D) were measured by flow cytometry following published procedures (Benedict *et al*., 1997). Experiments were repeated six times and arithmetic mean values $\pm$ standard error of the mean are reported. Data were fitted to the approximate equation $MFI = MFI_{max} \cdot [scFv]/(K_D + [scFv])$ using GraphPad Prism Software (GraphPad Software Inc., San Diego, CA, USA), where MFI is the mean fluorescent intensity and MFI_{max} is the fitted plateau value at high concentrations of scFv fragment.

Measurement of in vitro *serum stability*

The scFvs were separately incubated in human serum at concentrations of 1.5 μg/ml in a final volume of 30 μl at 37°C. After defined time periods of up to 4 weeks, the residual binding activity of the incubated scFvs was determined by flow cytometry. Binding was compared to samples withdrawn right after the incubation period had started, which were set to 100%. The experiment was repeated four times and the average half-life values were calculated from fitting to a monoexponential decay.

Equilibrium denaturation

A FluoroMax-4 spectrofluorometer (HORIBA Jobin Yvon, Inc., NJ, USA) was used to record fluorescence spectra at 25°C with slit widths of 2 nm for excitation and emission. Protein samples dissolved in guanidinium chloride (GdmCl) (1.0 ml) with a final protein concentration of 0.3 μM and denaturant concentrations from 0 to 5.0 M were prepared from a GdmCl stock solution (6.0 M, in 0.05 M Tris–HCl (pH 7.2), 100 mM NaCl). The final GdmCl concentration of each sample was calculated from its refractive index. Fluorescence emission spectra from 320 to 370 nm were recorded with an excitation wavelength of 280 nm after overnight incubation of the samples at 25°C. Fluorescence emission maxima were determined by fitting the fluorescence emission spectra to a Gaussian function, and plotted against the GdmCl concentration. Relative emission maxima were calculated by setting the highest value to 100 and the lowest to 0. Alternatively, fluorescence emission maxima were determined by fitting the fluorescence emission spectra with a Taylor expansion to the fourth power term according to (Monsellier and Bedouelle, 2005) as described in the Supplementary data available at *PEDS* online. Protein stabilities (ΔG, *m*-values) were evaluated by the linear extrapolation method according to published procedures (Santoro and Bolen, 1988; Jäger *et al*., 2001) but it was found that a two-state model does not hold.

Results

Homology modeling of 4G7-wt

The V_L domain of 4G7 is most likely derived from murine germline family muVκ2, presumably germline muVκ2–137 [IMGT database (Lefranc *et al*., 2005), AJ231263 (Schable *et al*., 1999), 98% sequence identity, 99% sequence similarity to 4G7] (Fig. 1), and was modeled against template structure 1MJU (96% identity, 98% similarity, 1.2 Å resolution) (Ruzheinikov *et al*., 2003). The high degree of sequence identity made modeling of this domain unproblematic, with only three amino acid substitutions in the putative antigen binding site and two in the framework: the fully exposed His L33 [All residue numbers are given in the AHo [(Honegger and Plückthun, 2001a) numbering scheme, in which structurally equivalent positions in V_L and V_H carry the same residue number. The correspondence between the AHo and the Kabat numbering schemes (Kabat *et al*., 1991) is indicated in the header of the sequence alignment (Fig. 1)] in CDR-L1 was replaced in the model by Asn, Leu L107 in CDR-L3 by Met, Phe L137 in CDR-L3 by Leu. Framework substitutions Val L11 Ile and Leu L147 Ile, compared to the template, both affected semi-exposed positions that could be accommodated in the model without additional adjustments.

To model the V_H domain of 4G7, derived from germline family muV_H1, presumably germline gene mVH-S136 (Lefranc *et al*., 2005) (AF304557, 91% identity, 93% similarity) (Fig. 1), multiple templates were used. PDB entry 1P7K [1.8 Å resolution, 86% sequence identity, 87% similarity (Schuermann *et al*., 2004)] was used as the primary template. In the region between Ser H7 and Cys H106, template and target sequences were identical. However, an additional template [1XGY, 2.7 Å resolution (Piscitelli *et al*., 2006)] had to be used to model the conformation of the N-terminal residues, since the N-terminal sequence of the V_H domain in structure 1P7K does not fit a muV_H1-derived sequence. With a glutamate in position H6 and a Pro in H10, 1P7K shows the sequence signature and conformation of a type I framework 1 kink conformation (Honegger and Plückthun, 2001b), while 4G7 shows the H6 Gln, H7 Ser, H10 Pro signature sequence of a type III kink. Such N-terminal sequence mismatches are frequently caused by the degenerate primers used for the cloning of antibody variable domains (Honegger and Plückthun, 2001b; Jung *et al*., 2001). Although these sequence differences were concentrated in the region from H1 to H6, they predominantly affect the framework backbone conformation in the region from H7 to H11. Therefore, the conformation of framework 1 residues H1–H22 was taken from template 1XGY. CDR-H3 and framework 4 of 4G7 were modeled using 1MNU [2.5 Å resolution (van den Elsen *et al*., 1999)] as template.

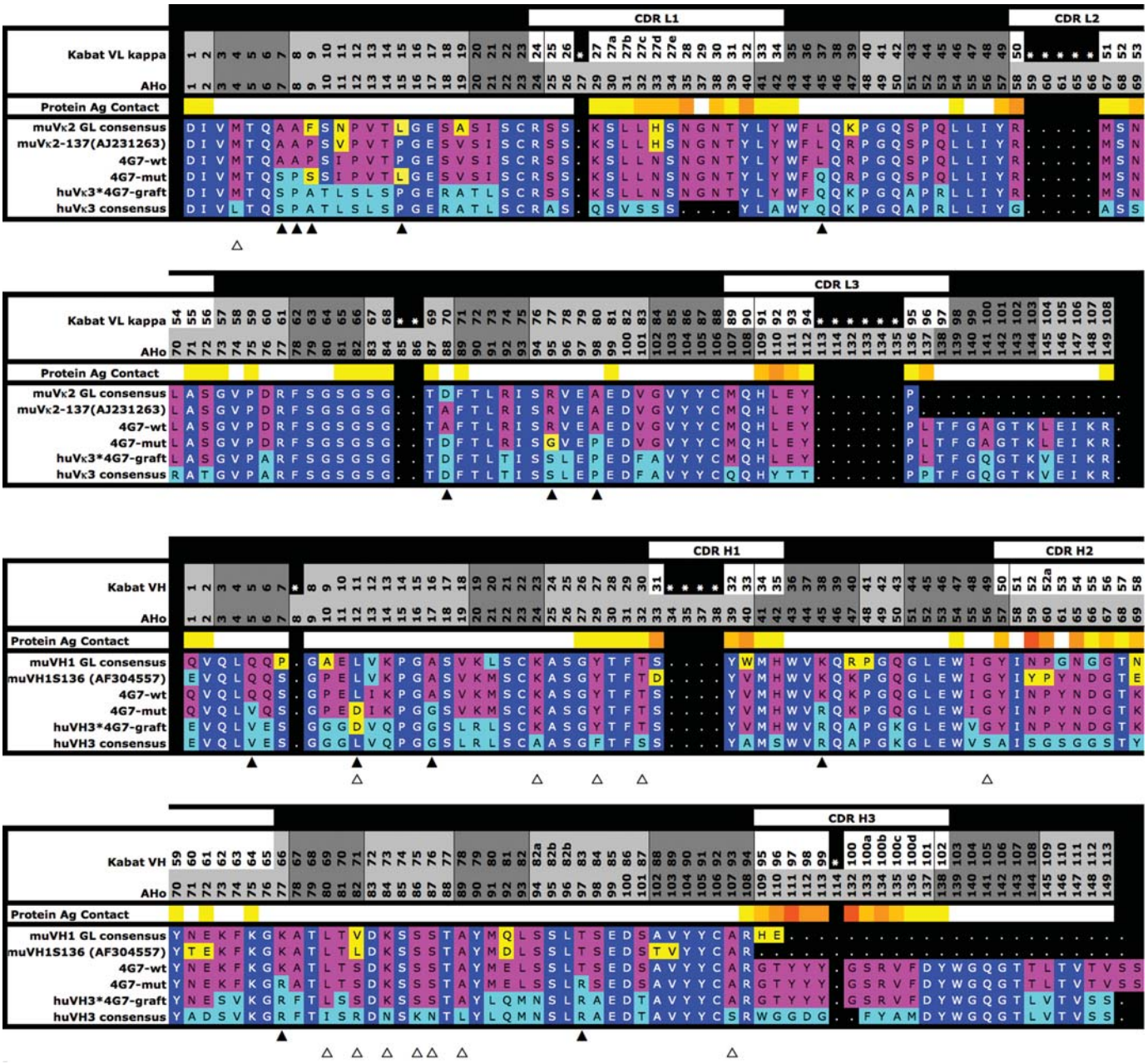

Fig. 1. Sequence alignment of the 4G7-wt V_L and V_H sequences (denoted *4G7-wt*) to their presumed parental germline precursors (*muVκ2-137(AJ231263)*, *muVH1S136 (AF304557)*) and germline family consensus sequence (*muVκ2 GL consensus*, *muVH1 GL consensus*), to the point mutant construct 4G7-mut (*4G7-mut*), the CDR-grafted variant 4G7-graft (*huVκ3*4G7-graft, huVH3*4G7-graft*) and the graft acceptor framework (*huVκ3 consensus*, *huVH3 consensus*) representing the human germline family consensus sequences for the huVκ3 and the huV$_H$3 families, with CDR-L3 and -H3 derived from humanized antibody hu4D5–8. In the header, the residue numbering according to Kabat *et al.* (1991) and AHo (Honegger and Plückthun, 2001a) are indicated, the extent of the CDRs according to the definition of Kabat *et al.* (1991) (white background) and the structurally least variant positions used for the least-squares superposition of variable domain structures (dark gray background). A color code (line *Protein Ag Contact*) indicates the probability of the different sequence positions to be involved in contacts to a protein antigen based on the average reduction of solvent accessible surface area (Honegger and Plückthun, 2001a): white; no contact, yellow; low probability to red; very high probability. Sequence positions identical in 4G7-wt and in huVκ3-huV$_H$3 are indicated in white letters on a dark blue background, sequence positions identical to 4G7-wt but different from huVκ3-huV$_H$3 by black letters on magenta, positions identical to huVκ3-huV$_H$3 and different from 4G7-wt by cyan, positions differing from either sequence are highlighted in yellow. Closed triangles point at sequence positions altered in 4G7-mut, open triangles at framework positions deviating from the sequence of the acceptor framework in 4G7-graft.

The two template Fvs were aligned by a least squares fit of the structurally conserved positions of both the V_L and the V_H domains, and the V_L domain model of 4G7 aligned to the V_L domain of 1MJU, the V_H domain model to the V_H domain of 1P7K, resulting in a relative domain orientation of the model intermediate between those of the two templates. Some adjustments in side-chain rotamers of residues in the V_L/V_H interface and in the CDR-H3 conformation were necessary to avoid steric clashes.

Identification of potentially destabilizing features in 4G7-wt

Sequence and structure model of 4G7 were scrutinized to identify potentially destabilizing features (Honegger, 2008)

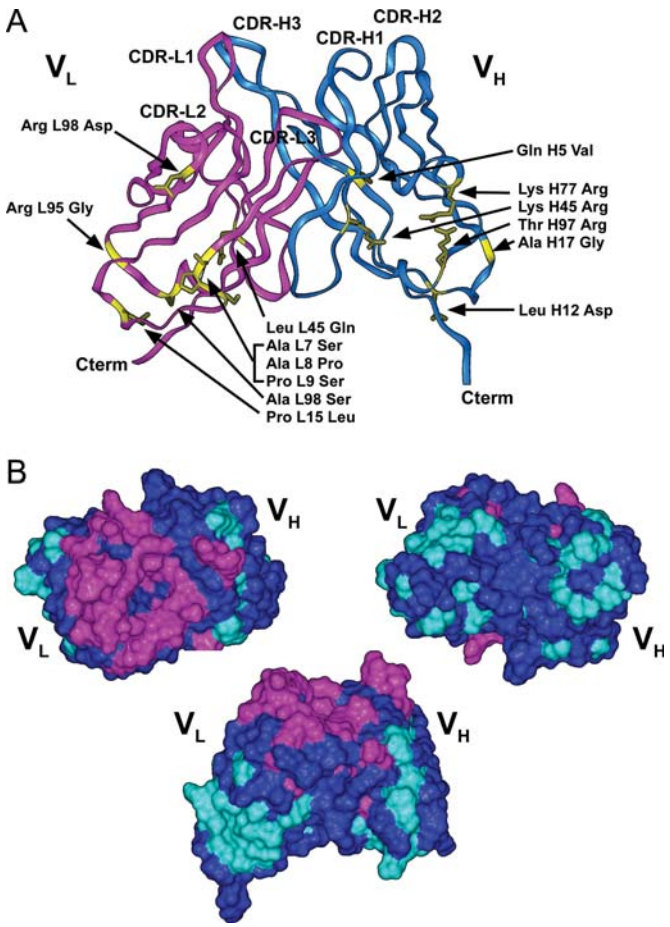

Fig. 2. Structural models of 4G7-mut and 4G7-graft. (**A**) Amino acid substitutions in 4G7-mut. The model structure of the scFv fragment shows the secondary structure of the V_L domain (magenta) and the V_H domain (blue). The 14 amino acid substitutions are highlighted in yellow, 8 in the V_L and 6 in the V_H domain. (**B**) Three-dimensional model of 4G7-graft. Residues derived from the CDR donor (murine 4G7-wt) are highlighted in magenta, residues derived from the framework donor (human V_H3 and Vκ3 domains) in cyan, and identical residues between both donors are highlighted in blue, respectively. Left: view from the 'top' (putative antigen binding site), right, view from the 'bottom' (in a Fab fragment, the V/C interface), bottom center: view from the 'front'.

(Figs 1 and 2A). Two principal problem spots became apparent in the 4G7-wt scFv.

Light chain positions l7, l8 and l9 forming the framework 1 kink The muVκ2 light-chain germline family shows an unusual conformation of the framework 1 kink between strand a′ and a″: Residue L8 is a *cis*-Pro in >99% of the human and 84% of the murine Vκ sequences. In muVκ2-derived V_L domains, L8 is an Ala, however, and L9 a *trans*-Pro. In the 4G7-wt sequence, L7 is an Ala, L8 an Ala, L9 a Pro. The presence of a *cis*-Pro in L8 has been shown to improve the folding behavior and stability of scFvs: from a library of an scFv fully randomized in positions L7, L8 and L9, the S-P-S amino acid combinations most frequently seen in natural antibodies also prevailed (Spada *et al*., 1998). Sequences containing Pro in position L8 were preferred over other amino acids in this position and were produced with a higher yield of native protein upon periplasmic expression. Reanalysis of the raw data (Spada *et al*., 1998) showed that all of the selected clones showing a Pro in position L9 also had a Pro in L8, contrary to the situation observed in 4G7. Similarly, in an *in-vitro* evolution experiment aimed at increasing the stability of the disulfide-free scFv AB48, clones containing the mutation from T-T-S to T-P-S were generated and enriched (Proba *et al*., 1997; Proba *et al*., 1998). Surface residue Ser L7, present in 96% of human and 70% of murine Vκ sequences, forms a hydrogen bond to its own main chain CO, facilitating the formation of the chain kink between strands a′ and a″. Of the sequences lacking this Ser, the majority have a Thr in this position that can also form this hydrogen bond. In the point mutation construct 4G7-mut, we therefore replaced the L7-L9 AAP motif of 4G7 by SPS.

Heavy chain position H45, H77 and H97 in the charge cluster In antibody variable domains, a highly conserved cluster of charged residues is buried or semi-buried in the lower core of the domain. Arg H77 and Asp H100 form the central core of this cluster, interacting in a doubly hydrogen-bonded salt bridge. Charged residues Arg H45, Glu H53, Arg H97 and Glu H99 surround this central salt bridge to form the charge cluster, while highly conserved Tyr H104 helps to orient the Asp H100 side chain by forming a hydrogen bond to its main-chain carbonyl group. While 86% of all human V_H domains have an arginine in position H77, 56% of the murine V_H sequences have a lysine residue in this position. Such domains are significantly stabilized by having Arg H77 instead of Lys (Lindner *et al*., 1997; Proba *et al*., 1997; Proba *et al*., 1998; Wörn *et al*., 2000). The Arg H97-Glu H99 ion pair is more solvent-exposed than the Arg H77-Asp H100 salt bridge. However, the interaction of Glu H99 with Arg H87 and with Arg H45 probably keeps the glutamate from interacting with Arg H77 and thus from opening up the charge cluster to the solvent. In 4G7-wt, H45 and H77 are both lysines, H97 a threonine. In 4G7-mut, we therefore replaced the three residues with arginines to optimize the charge cluster.

Surface mutations with a track record Besides these two major problem spots described above, a few minor changes of surface residues were introduced that had proven beneficial in other antibody fragments: residue L15 is part of a semi-buried cluster of hydrophobic amino acids. The substitution of Ala L15 by Leu stabilized the MCPC603 V_L domain by 7.0 kJ/mol, Ala L15 Pro by 4.5 kJ/mol (Ohage *et al*., 1997); the inverse substitution of Leu L15 by Pro destabilized the LEN V_L domain by 7.1 kJ/mol (Raffen *et al*., 1999). In 4G7-mut, we therefore replaced Pro L15 by Leu.

H5 is a fully exposed surface residue. However, the well-expressed huV$_H$3, huV$_H$1 and huV$_H$5 human germline consensus frameworks have a Val in this position (Ewert *et al*., 2003b), while the poorly expressed huV$_H$2, huV$_H$4 and huV$_H$6 have a Lys (V_H2) or Gln (V_H4, V_H6) in this position. The mutation of Gln to Val in two different antibodies derived from the human V_H6 germline family resulted in 1.7- and 2.6-fold increase in production yield (soluble periplasmic protein) and a stabilization shifting the midpoint of the GdmCl denaturation curve ($[GdmCl]_{50}$) by 0.1 and 0.15 M, respectively (Ewert *et al*., 2003a). In addition, H5 Val was selected over Gln, Leu and Glu in the phage display selection of 4D5-Flu for improved stability (Jung *et al*.,

1999). A possible reason for the beneficial effect of Val in this solvent-exposed position lies in the particularly high β-sheet propensity of β-branched amino acids, which might help to stabilize the short N-terminal a′ β-strand of the immunoglobulin variable domain. We therefore replaced Gln H5 of 4G7-wt by Val in 4G7-mut.

Hydrophobic surface residues in the V_H/C_H interface of the Fab fragment are solvent exposed in scFvs, where they can have a negative influence on the folding efficiency of an scFv. In the anti-fluorescein antibody 4-4-20, the substitution of Leu H12 by Ser had no significant effect, while the substitution of Leu H12 by Asp significantly improved the production yield (Nieba *et al*., 1997). We therefore replaced Leu H12 by Asp both in 4G7-mut and in the 4G7-graft.

Additional mutations The changes suggested above had been tested in other scFvs and shown to improve stability and/or folding efficiency without affecting antigen binding. Additional mutants were suggested based on sequence statistics and structural criteria.

Position L45 in V_L corresponds to H45 in the heavy chain and is likewise in contact with the charge cluster in the lower core of the domain. In 4G7-wt, L75 is a Leu, while 88% of human and 78% of murine antibodies have a Gln in this position. The huVκ1 and huVκ3 consensus domains have a Gln in this position, the less well-behaved huVκ2 a Leu (Ewert *et al*., 2003b). In 4G7-mut, we placed a Gln in this position.

Sequence statistics indicate a strong preference for Asp in position L88. Mutations from the germline consensus Asp to His or Asn in human Vκ1-derived light chains have been reported to increase propensity for amyloid formation (Stevens *et al*., 2000). However, an effect of this mutation on antigen affinity cannot be excluded, since in protein-binding antibodies the outer loop of V_L may make contact to the antigen. Ala L88 was nevertheless replaced by Asp, and did not have a deleterious effect on binding (see below).

Residue L95 frequently has a positive Phi torsion angle. Arg L95 was therefore replaced by Gly in 4G7. For the same reason, Ala H17 was replaced by Gly. H17 is a Gly in the very stable huV$_H$3 consensus domain (Ewert *et al*., 2003b), and in IcaH-01, the substitution of Ala H17 by Gly stabilized V_H with a shift in $[GdmCl]_{50}$ by 0.1 M (Wirtz and Steipe, 1999).

In the majority of murine Vκ domains, an Ala is found in position L98, as it is in 4G7-wt. In human Vκ domains, Pro predominates. In the *in vitro* evolution of the 4D5Flu scFv towards improved stability, Pro was selected over Ser and Ala (Jung *et al*., 1999) in this position. In addition, replacement of Pro by other residues in Vκ1 was reported to be linked to increased propensity for the formation of amyloid (Stevens *et al*., 2000). Therefore, we replaced Ala L98 by Pro.

As a result of this analysis, 14 point mutations were introduced into the 4G7-wt scFv to yield the scFv 4G7-mut (Figs 1 and 2A).

Design of the CDR graft 4G7-graft

In designing a CDR graft from a murine to a human antibody, one often has the choice of either grafting to the human acceptor framework that is closest to the sequence of the CDR donor, or to an acceptor framework with proven good biophysical characteristics. The sequence of the V_L domain of 4G7 most closely resembles that of huVκ2, with 79% sequence identity and 84% similarity. However, the huVκ2 consensus fragment shows relatively poor biophysical characteristics (Ewert *et al*., 2003b). The V_H domain of 4G7 most closely resembles huV$_H$1, with 73% identity and 79% similarity. Based on the analysis of Ewert *et al.* (2003b), who performed a detailed biophysical characterization of a series of consensus frameworks representing the major human germline families, huVκ3 is the most stable human Vκ fragment, huV$_H$3 the most stable human V_H fragment. We therefore chose this framework combination as acceptor framework, despite the fact that huVκ3 showed a mere 53% sequence identity and 65% similarity to the V_L domain of 4G7 and huV$_H$3 51% identity and 65% similarity to the V_H domain of 4G7 (Fig. 1).

To model the CDR graft, the V_L and V_H 4G7-wt domain models were aligned to the corresponding domains of a previously built model of the huVκ3-huV$_H$3 Fv fragment (Knappik *et al*., 2000). Starting from the superposed models of the acceptor framework and the CDR donor, a model of the graft was built, combining the coordinates of the loops containing the CDRs and the outer loops from the model of the CDR donor with the rest of the coordinates from the model of the acceptor framework. The cut-points between the two models were placed within the adjacent β-strands forming the structurally least variable regions in antibody variable domains, marked by dark gray boxes in Fig. 1. This allowed the fragments of the model to be joined without introducing undue strain. Sequence positions that were identical in both sequences (marked in dark blue in the sequence alignment) did not have to be changed. Since no experimental structure of the complex of 4G7 with its antigen was available, potential antigen contact residues were identified by an extensive analysis of known complexes of antibodies with protein antigens (Honegger and Plückthun, 2001a) (see Supplementary data available at *PEDS* online for additional information). These sequence position, marked as 'Protein Ag Contact' in the header of the sequence alignment (Fig. 1) were changed to the sequence of the CDR donor. In addition, the buried residues that pack the space between the CDRs and a highly conserved layer of residues across the domain core (Cys 23 and Cys 106, Trp 43, Thr 143) were changed to the sequence of the CDR donor to avoid destabilization of the desired CDR conformation. Residue L4 was changed from the Leu of the acceptor framework to Met found in the CDR donor. Buried Ala L24 was replaced by the Ser of the CDR donor, since this substitution can influence the conformation of CDR-L1. H1 was kept a Glu, and H24 Ala, H29 Phe and H32 Ser adjacent to CDR-H1 were likewise adjusted to the 4G7 CDR-donor sequence. L44 was kept a Phe like in 4G7 instead of Tyr in the acceptor framework. Located in the V_L/V_H interface, L44 has been observed to contact the antigen in hapten and peptide binding antibodies, and could potentially affect the relative domain orientation.

Optimization of the packing interactions between CDR-H2 and framework residues is critical to the success of a CDR-graft to a framework of divergent subtype. Position H56 adjacent to CDR-H2 is a buried Ser or Ala in huV$_H$3, Gly in most other V_H domains, including 4G7. Since this sequence difference affects the local β-bulge backbone conformation, it was also adjusted to the 4G7 sequence. In contrast, residues H73 and H74 were changed to the sequence of the framework donor, since in particular H74 interacts with the hydrophobic

core of the framework. Interacting residues H74 and H78 are Phe and Ala in 4G7, yet Val and Phe in huV$_H$3. The combination of two Phe residues in the graft would have overpacked the core of the domain, which would either result in significant destabilization or a change in the CDR-H2 takeoff angle.

The outer loop of the V$_H$ domain (H83-H88) is relatively variable in structure. In contrast to the corresponding loop in V$_L$, it has not been observed to directly contact the antigen, but it can affect CDRs -H1 and -H2. Outer loop residues H80–H89 were thus retained from the 4G7 sequence, since buried residues H80 and H89 pack against buried CDR-H2 and CDR-H1 residues. H107, adjacent to CDR-H3, was likewise taken from 4G7. All other residues were taken from the acceptor frameworks, with the exception of exposed Leu H12 in the former V$_H$/C$_H$ interface, which was replaced by an Asp (Fig. 2B) in 4G7-graft as well as in 4G7-mut, since it can have a marked effect on folding efficiency.

4G7-mut has higher soluble expression yields than the other two variants

The 4G7-scFv variants were expressed in *E.coli* HB2151 and purified from periplasmic extracts by NiNTA affinity chromatography and ion exchange chromatography (Fig. 3B and C). scFv purification yields were determined by densitometry of Coomassie stained SDS–PAGE gels (Table I). 4G7-mut was expressed consistently with about 2-fold higher yields than 4G7-wt and 4G7-graft (2.3 ± 0.8 mg/l versus 1.2 ± 0.3 and 1.1 ± 0.2 mg/l, respectively), corresponding to 135 ± 15 μg scFv per gram wet weight *E.coli*, 92 ± 16 and 80 ± 28 μg/g, respectively. These data suggest that the mutations of 4G7-mut indeed lead to an improved folding efficiency due to the 14 mutations.

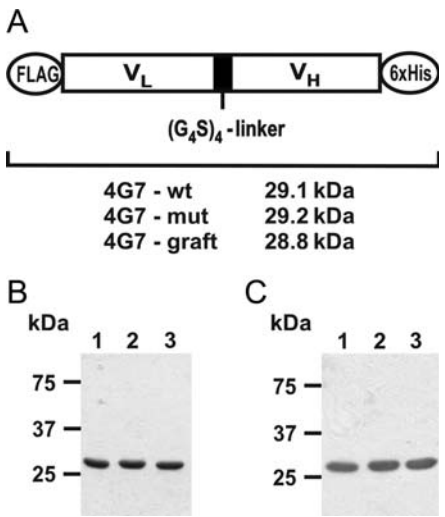

Fig. 3. scFv construct and purification of the three 4G7 variants. (**A**) *FLAG*, N-terminal FLAG-tag; *6xHis*, hexahistidine tag; V_L and V_H, variable domains of light and heavy chains of the 4G7-scFv connected by a (Gly$_4$Ser)$_4$ linker; molecular masses of 4G7-wt (29.1 kDa), 4G7-mut (29.2 kDa) and 4G7-graft (28.8 kDa) were calculated from their amino acid sequences. (**B** and **C**) Periplasmic expression and purification of the 4G7 scFvs by IMAC and subsequent ion exchange chromatography. Purified proteins were analyzed by SDS–PAGE and (B) Coomassie staining or (C) western blot using a primary Penta-His antibody. Lanes 1–3: 4G7-wt, 4G7-mut, 4G7-graft.

Table I. Biophysical properties of 4G7 scFv variants

scFv	Soluble yield		Binding affinity	Serum half-life
	(mg/l *E.coli)*	(μg/g *E.coli)*	nM	h
4G7-wt	1.2 ± 0.3	80 ± 28	8.4 ± 0.9	95
4G7-mut	2.3 ± 0.8	135 ± 15	16.4 ± 1.6	106
4G7-graft	1.1 ± 0.2	92 ± 16	30.0 ± 2.7	82

All three scFv variants show similar behavior in analytical gel-filtration

To analyze the tendency of the purified scFvs for forming aggregates, analytical gel-filtration experiments were performed (Fig. 4). For 4G7-wt, ~92% of the protein eluted at the expected size for a monomer, ~8% at the size expected for a dimer and no higher aggregates were seen. The elution profiles for 4G7-mut and 4G7-graft contained ~11.5 and ~12.5%, respectively, of protein with the mobility of dimers. Dilution of the sample to 0.25 mg/ml and 5 hours incubation before measurement did not alter the fraction of dimers. Multi-angle light scattering (MALS) measurements allowed us to determine the molecular masses of the faster eluting material, which were consistent with the interpretation of dimers. The values measured by MALS for the monomer and presumed dimer peaks for 4G7-wt were 29.7 ± 0.6 and 66.0 ± 5.9 kDa; for 4G7-mut: 29.4 ± 0.6 and

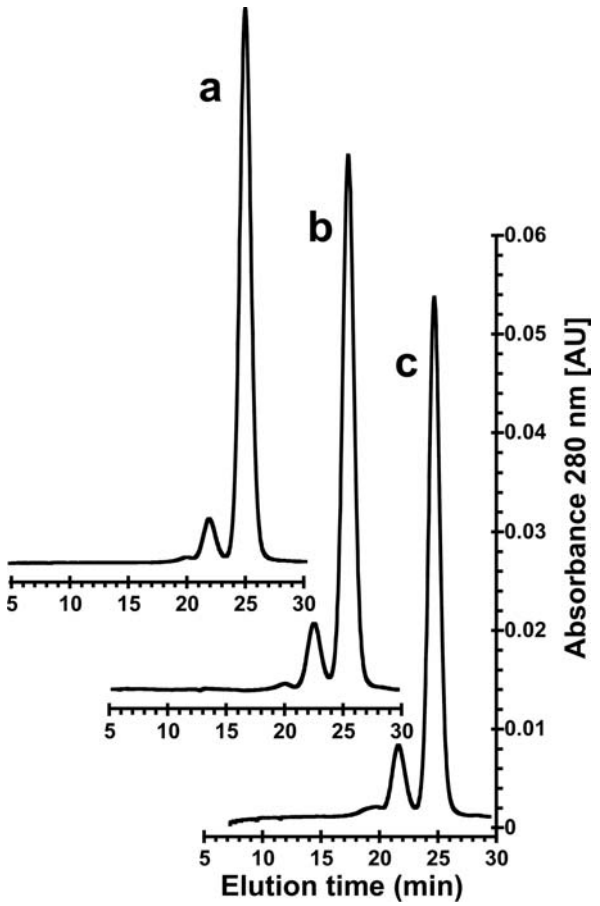

Fig. 4. Analytical gel-filtration of 4G7 variants. Samples (applied at a concentration of 0.5 mg/ml (17 μM) were analyzed on a Superdex-75 column in 50 mM sodium phosphate (pH 7.0), 100 mM NaCl with 4G7-wt (**A**), 4G7-mut (**B**), and 4G7-graft (**C**).

62.2 ± 3.1 kDa; and for 4G7-graft: 29.4 ± 0.6 and 60.0 ± 2.4 kDa. The two different design principles used to produce the 4G7-mut and -graft variants, therefore, had no significant effects on the propensity of these variants to form dimers.

4G7-mut has the greatest thermodynamic stability, determined by equilibrium denaturation

Thermodynamic stabilities of the three variants were assessed by denaturant-induced equilibrium denaturation/renaturation experiments. To this end, the proteins were incubated in the presence of various concentrations of guanidinium chloride (GdmCl) overnight at 25°C, and fluorescence emission spectra were measured in the wavelength range from 320 to 370 nm, using an excitation wavelength of 280 nm. Each of the three constructs contained four tryptophan residues contributing to the fluorescence spectrum: Trp L43 and Trp H43 located in the core of the V_L and the V_H domain usually are quenched by the neighboring disulfide bond in the native state, while Trp H54 and Trp H149, buried in the V_L/V_H dimer interface, make a strong contribution to the fluorescence signal of the native scFv. 4G7 (and all the variants) contained only these four highly conserved tryptophans, with no additional Trp in the CDRs.

While the wavelength of the fluorescence maximum of the native 4G7-graft (338.6 nm) was close to that of the full consensus huVκ3-huV$_H$3 (338.7 nm), the fluorescence maxima of 4G7-wt (342.0 nm) and 4G7-mut (340.8 nm) were consistently red-shifted by 2–3 nm relative to 4G7-graft (Fig. 5). To ensure that this shift was not due to the presence of a dimer species with different spectral properties, the spectra of the monomer and dimer fractions were measured immediately after their elution from the gel filtration column. Indeed, the same 2–3 nm shift was seen between the monomer of 4G7-graft and the monomers of the other two constructs, while no significant difference was detected between the spectra of the monomer and the corresponding dimer. Therefore, this shift seems indeed to be due to the difference in the intrinsic spectral properties of the native molecules, not to the presence of aggregated or misfolded species.

The equilibrium unfolding/refolding curves were evaluated by a two-state fit (Santoro and Bolen, 1988) (Fig. 5). Additional details are shown in the Supplementary data available at *PEDS* online. Based on the homology models of the Fv fragments, an *m*-value of 5.6–5.9 kcal·mol/l^2 would be predicted (Myers *et al*., 1995). The *m*-values of 2.1–2.6 kcal·mol/l^2 derived from the two-state fit for 4G7-wt, 4G7-graft and for the acceptor framework huVκ3-huV$_H$3, representing the germline family consensus for the two domains (Knappik *et al*., 2000), with CDR-L3 and -H3 taken from hu4D5–8 (Eigenbrot *et al*., 1993), are far too low for a protein the size of an scFv containing two disulfide bonds. This indicates that the unfolding transition does not really represent a two-state transition, and the extrapolation to zero denaturant concentration inherent in the calculation of $\Delta G_{(H2O)}$ is not reliable. It is particularly problematic to compare fragments with strongly different apparent *m*-value, even qualitatively. Such a deviation from two-state unfolding behavior is not unusual for antibody scFvs, which, depending on the intrinsic stabilities of the domains and the stability difference between V_L and V_H domain, may show anything from a fully cooperative unfolding of the two domains to the formation of stable equilibrium unfolding intermediates, in which one domain is still native while the other is fully denatured (Wörn and Plückthun, 1998; Jäger *et al*., 2001). Similar deviations from two-state behavior have also been observed in the scFv analyzed in the accompanying paper (Honegger *et al*., 2009) and are discussed in detail in the Supplementary data available at *PEDS* online for that paper. We also discuss there why incomplete unfolding at high denaturant concentrations—which in principle can lead to low *m*-values—would not be consistent with our data.

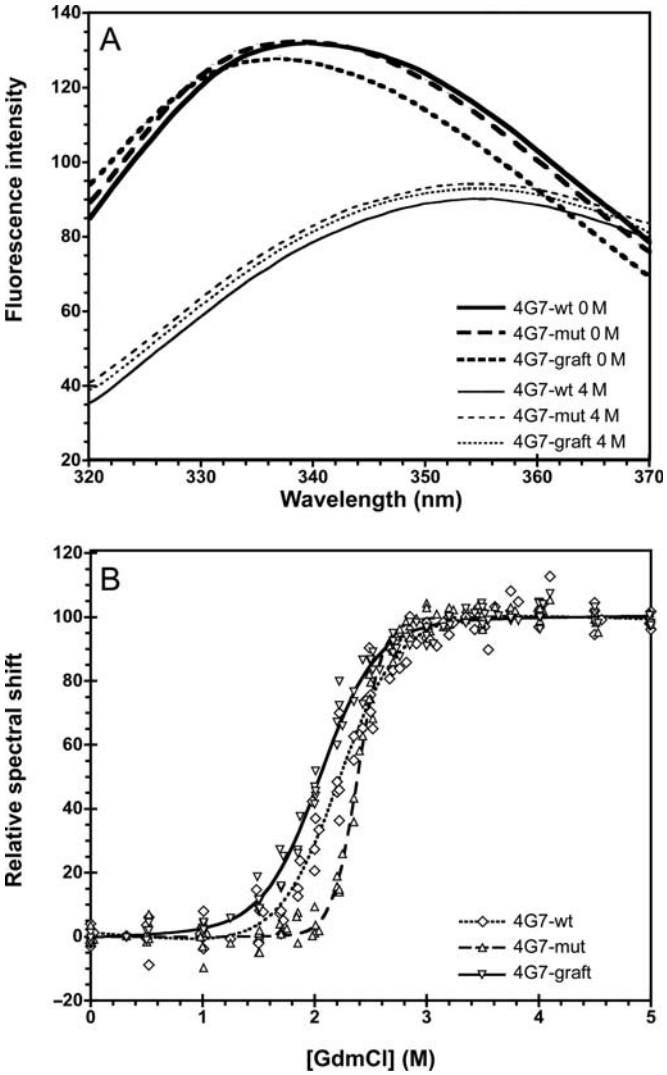

Fig. 5. GdmCl equilibrium denaturation of the 4G7 variants. (**A**) Fluorescence spectra of native and unfolded (in 4 M GdmCl) 4G7 variants. (**B**) Equilibrium denaturation curves of constructs 4G7-wt, 4G7-mut and 4G7-graft. The unfolding transitions were observed by following the change of the wavelength of the emission maximum of the Trp fluorescence (excitation wavelength 280 nm) as a function of denaturant concentration. The actual shift can be seen in (A), and it is expressed here as a percentage from 0 (maximum of the native state) to 100 (maximum of the denatured state). The data were fitted using the two-state model (Santoro and Bolen, 1988) for illustrative purposes only, simultaneously fitting the pre-transition-baseline (λmax_N, m_N), the post-transition baseline (λmax_U, m_U) and the thermodynamic parameters $\Delta G_{(H2O)}$ and *m*, and plotted as relative spectral shift (relative change of λmax_{obs} versus denaturant concentration) after baseline correction (see Supplemental data available at *PEDS* online, Table ST3). However, as explained in the text, and in more detail in the Supplementary data available at *PEDS* online, the low *m*-values obtained for 4G7-wt and 4G7-graft indicate that the two-state assumption is not fulfilled, and the fitted $\Delta G_{(H2O)}$ values would be meaningless.

The higher apparent cooperativity of 4G7-mut (*m*-value of 5.3 kcal·mol/l^2) indicates that it more closely approaches the behavior of a two-state system. This effect is found when the difference between the intrinsic stabilities of the two domains has been reduced and there is significant mutual stabilization between the domains (Wörn and Plückthun, 1998; Jäger *et al*., 2001; Honegger *et al*., 2009). In 4G7-mut, the shift to a higher $[GdmCl]_{50}$ shows that the weaker domain has been stabilized to a larger degree than the stronger one. This is consistent with the weaker domain having become intrinsically more stable. While increased mutual stabilization of the two domains would also lead to increased cooperativity with concomitant shift to a higher $[GdmCl]_{50}$, none of the mutations is located in the V_L/V_H interface, and thus, this is less likely to be responsible for the observed increase of the m-value.

While it was not possible to derive the absolute stabilities of the constructs from such measurements, qualitatively, the stabilities of the constructs can be ranked based on the midpoints of the transition curves (Fig. 5B). This merely assumes that the ranking in the absence of denaturant follows the ranking at intermediate denaturant concentration. With a midpoint of 2.4 M, 4G7-mut is the most stable of the three 4G7 variants. Amongst the three constructs, it is the one whose denaturation starts at the highest denaturant concentration. Despite the fact that the acceptor framework huVκ3-huV$_H$3 with a midpoint of 2.8 M is more stable than any of the 4G7 variants, the graft of the 4G7 CDRs to the huVκ3-huV$_H$3 framework has a denaturation midpoint of only 2.1 M, and is therefore slightly less stable than the murine wild-type, 4G7-wt with 2.2 M.

All three variants have similar functional stability in human serum

To measure their stability in human serum, all three variants were incubated in serum at a concentration of 1.5 μg/ml at 37°C for different lengths of time before residual binding was measured by flow cytometry. Staggered starting times and a common endpoint were used, and a sample of scFv freshly added to serum was then used to define 100% binding at t_0. All values were normalized to this t_0-value (Fig. 6 and Table I). The serum half-lives do not differ greatly, with that of 4G7-mut being slightly higher with 106 h, compared to wt with 95 h and 4G7-graft with 82 h, respectively. The reported half-lives represent the averages of four independent measurements.

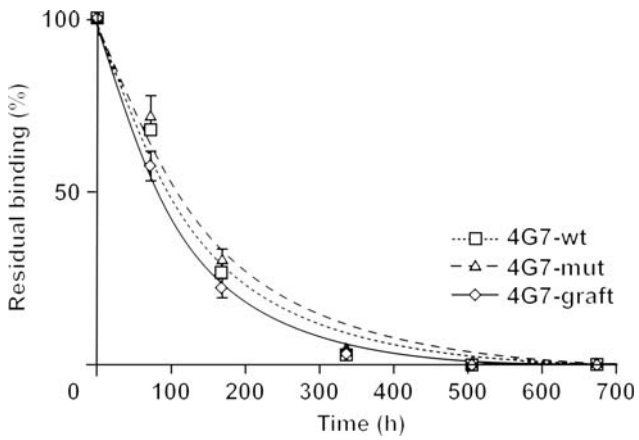

Fig. 6. Serum stability of 4G7 variants at 37°C. ScFvs were incubated in human serum at 37°C for the time periods indicated. The residual binding activities of purified 4G7-wt (squares), 4G7-mut (triangles) and 4G7-graft (diamonds) variants were determined by flow cytometry on CD19-positive SEM cells. The data are expressed as a percentage of the sample at t_0 (taken immediately after addition of scFvs to human serum) and present the mean percentage of residual binding ± standard error of the mean of four independent experiments. Serum half-lives ($t_{1/2}$ values) deduced from these curves are reported in Table I.

All variants retain antigen-specific binding, but 4G7-graft has a slightly lower affinity

All three variants bound to CD19-positive SEM leukemic cells in an antigen-specific manner (Fig. 7). They bound to antigen-positive cells (Fig. 7A, C and E), but not to antigen-negative cells (not shown), and binding was blocked by pre-incubation of the cells with a 50-fold molar excess of the parental antibody 4G7 (Fig. 7B, D and F), but not by a corresponding molar excess of an isotype control antibody, which itself did not react with CD19 (not shown). Therefore, introduction of the 14 point mutations and the grafting procedure apparently have not introduced any unspecific binding property into the variants.

Binding affinities were determined by an immunofluorescence assay, in which increasing concentrations of the scFvs were incubated with constant numbers of CD19-positive SEM cells. Equilibrium constants (K_D) were determined from a fit of the mean fluorescence intensity to a 1:1 saturation model. The 4G7-wt had an affinity of $K_D = 8.4 \pm 0.9$ nM, and 4G7-mut gave a value of 16.4 ± 1.6 nM, while

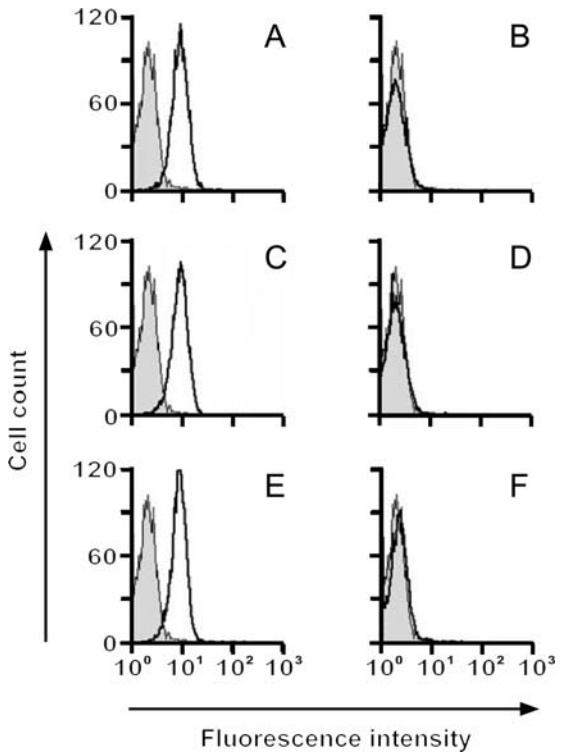

Fig. 7. Specific binding of 4G7 variants to CD19-positive cells. (**A** and **B**), 4G7-wt; (**C** and **D**), 4G7-mut; (**E** and **F**), 4G7-graft. Flow cytometric analysis was performed by staining cells with equal concentrations of purified CD19-specific scFvs (black line) or a non-related scFv (light gray) (A, C, E). For competition experiments (B, D, F), cells were pre-incubated with a 50-fold molar excess (black line) of parental 4G7 mAb. Pre-incubation with a non-related mAb did not block binding of the 4G7 scFvs (data not shown).

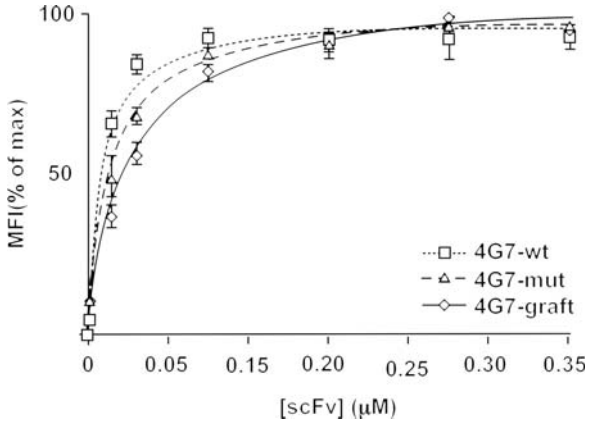

Fig. 8. Determination of equilibrium binding constants of 4G7 variants on CD19 bearing cells. CD19 positive SEM cells were incubated with increasing concentrations of purified 4G7-wt (squares), 4G7-mut (triangles) and 4G7-graft (diamonds). Cell-bound scFvs were detected by staining with a secondary PE-conjugated antibody and analyzed by flow cytometry. The mean fluorescence intensity (MFI) is plotted as a percentage of its maximal plateau value, and the K_D is estimated by $MFI = MFI_{max} \cdot [scFv]/(K_D + [scFv])$. Averaged over 6 independent experiments, the K_D values were 8.4 ± 0.9 nM, 16.4 ± 1.6 nM, and 30.0 ± 2.7 nM for 4G7-wt, 4G7-mut and 4G7-graft, respectively.

4G7-graft gave 30.0 ± 2.7 nM, indicating a slight effect of the framework on the CDRs (Fig. 8 and Table I).

Discussion

This study aimed at comparing two orthogonal strategies for improving the stability and expression yield of a scFv, using a CD19-specific scFv derived from murine monoclonal 4G7, an antibody with very favorable biological properties as an example. To this effect, two variants of 4G7-wt were constructed: 4G7-mut with 14 single amino acid substitutions at selected critical positions, and 4G7-graft with the murine CDR sequences grafted to a human framework. These variants were produced and analyzed in parallel with the wt protein, and two main results were obtained: first, 4G7-mut had approximately 2-fold greater expression yields and greater thermodynamic stability than the wt (which turned out to be on the upper end of the usually observed values for murine antibodies), and an almost identical affinity (2-fold). Second, the 4G7-graft had approximately equal yield and thermodynamic stability as the wt, but also a 3–4-fold reduced affinity.

The variants did thus not differ dramatically in their properties from the wt, less than expected from the design, and therefore, these results require some comments. The murine wt scFv already had comparatively favorable properties, and thus this study concentrated on testing whether they can be improved even further.

CDR-grafts, the transfer of the antigen binding loops from an antibody with a desired antigen specificity to a different antibody framework for the dual purpose of increasing the stability and reducing the immunogenicity of an antibody construct, represent by now a routine technique in antibody engineering. The huVκ3 and huVκ1 germline consensus for the V_L domain and the huV$_H$3 germline consensus for the V_H domain are the most frequently used human acceptor frameworks, both because they represent the most frequently utilized germline families in the human antibody repertoire and because these consensus domains show the most favorable biophysical properties (Ewert *et al*., 2003b). However, while CDR grafts from problematic antibody scFvs to these stable frameworks usually yield chimeric scFvs of greater stability than the CDR donor, they frequently fail to reach the level of stability observed for the consensus frameworks themselves (Willuda *et al*., 1999). This reduced stability could be due to destabilizing interactions within the CDRs or between CDRs and framework. In the consensus scFv used for comparison (Knappik *et al*., 2000; Ewert *et al*., 2003b), CDR-1 and -2 sequences were derived from the same V-gene consensus as the framework sequences themselves, and thus presumably represent an optimal fit to these frameworks, while in a CDR graft, and especially in a CDR graft from a highly divergent framework, a mismatch between CDRs and framework may lead to a destabilization of the individual CDR-grafted domains (Honegger *et al*., 2009) (accompanying paper). In addition, the CDRs contribute to the interface between the V_L and the V_H domain and, therefore, to the degree of mutual stabilization between the two domains (Wörn and Plückthun, 1998; Röthlisberger *et al*., 2005).

In this study, we compared the biophysical properties of an scFv derived from the murine monoclonal antibody 4G7 (4G7-wt) both to those of a variant in which a number of destabilizing features in the 4G7 framework have been repaired by point mutations (4G7-mut) and to those of a variant in which the CDRs of 4G7 have been grafted to the frameworks of the most stable human consensus domains, huVκ3 and huV$_H$3 (4G7-graft). With a $[GdmCl]_{50}$ of 2.2 M, the murine 4G7-wt scFv is already quite stable in equilibrium denaturation, e.g. compared to the hu4D5-8 scFv (Herceptin) (Eigenbrot *et al*., 1993), which is itself a CDR-graft. hu4D5–8 scFv shows a first step of equilibrium denaturation, the unfolding of the V_H domain, with a $[GdmCl]_{50}$ of only 1.4 M (Jäger *et al*., 2001), even though it expresses well and is not aggregation prone. Indeed, the hu4D5-8 scFv shows significantly lower stability than its own human consensus acceptor framework, huVκ1-huV$_H$3. This acceptor, even with CDR-L3 and -H3 derived from hu4D5-8, unfolds with a $[GdmCl]_{50}$ of 2.8 M (Ewert *et al*., 2003b), pointing to an important role of CDR-1 and CDR-2 in stability.

The acceptor framework used in the construction presented here, huVκ3-huV$_H$3, has a $[GdmCl]_{50}$ of 2.6 M (Honegger *et al*., 2009) to 2.8 M (Ewert *et al*., 2003b). The CDR-graft 4G7-graft with a $[GdmCl]_{50}$ of 2.1 M turned out to be slightly less stable than the parental murine scFv 4G7-wt. The *m*-values (cooperativity) of the equilibrium unfolding transitions of 4G7-wt, 4G7-graft and of the acceptor framework huVκ3-huV$_H$3 were all significantly lower than expected for a protein the size of an scFv containing two disulfide bridges, indicating deviation from a two-state transition, and this is why we resort to reporting $[GdmCl]_{50}$ and not ΔG values. These $[GdmCl]_{50}$-values are to be understood as qualitative midpoints of the unfolding trace, since the presence of a hidden intermediate does not allow to quantify the fraction of molecules that are unfolded at a given GdmCl concentration. This low apparent *m*-value can be explained by the scFv showing a difference between the intrinsic stabilities of the V_L and the V_H domain large enough that the

stabilizing influence of the V_L/V_H interface is insufficient to enforce fully cooperative unfolding of the scFv. This point is illustrated in the Supplementary data available at *PEDS* online, of this paper and the accompanying manuscript (Honegger *et al*., 2009).

While various additional mutations outside the classical CDR boundaries have been introduced in order to preserve the upper core packing of the CDR donor in the graft and to minimize steric conflicts between framework and CDR residues that potentially could alter the CDR conformation or destabilize the scFv, the high stability of the human acceptor framework (with its own CDRs) could not be maintained. This is due to residual strains between the grafted CDRs and the acceptor framework, similarly found in the Herceptin construct itself and in a case described in the accompanying paper (Honegger *et al*., 2009).

In the second approach presented here, we addressed individual destabilizing features in the 4G7-wt sequence with a series of point mutations located within the frameworks of the two domains. In a knowledge-based approach, we scanned the sequence of 4G7-wt against our database of mutations known to affect the stability and/or folding efficiency of antibody variable domains, and we identified 14 positions requiring mutation. Ten of these mutations are mutations towards the huVκ3 or the huV$_H$3 sequence consensus and thus are also present in 4G7-graft. One of the mutations, the replacement of hydrophobic surface residue Leu H12 by Asp, was also introduced in 4G7-graft, since this mutation had previously been shown to have a beneficial effect on the folding efficiency of scFv without affecting stability (Nieba *et al*., 1997), increasing the ratio of soluble protein to aggregates in the periplasm. The largest effect on stability was expected from the optimization of the charge cluster in the lower core of the V_H domain (position H77, H45 and H97). Other mutations were targeted at optimizing the framework 1 kink of the V_L domain and at non-Gly positions that carry positive phi angles in a majority of the known antibody structures.

With a $[GdmCl]_{50}$ of 2.4 M, 4G7-mut turned out to be the most stable of the three 4G7 constructs. In addition, the significantly increased cooperativity indicates that by predominantly stabilizing the weaker of the two domains, we succeeded in reducing the difference between the intrinsic stabilities of the V_L and V_H domains. Measures of serum half-life, production yield and ratio of the production of soluble protein to aggregates in the periplasm of *E.coli* all favored 4G7-mut over 4G7-wt and 4G7-graft.

The observation that a limited number of point mutations in the framework was capable of stabilizing 4G7-wt, while a graft to the most stable human consensus framework combination failed to do so, suggests that the relatively low stability of the graft cannot be blamed on destabilizing influences located within the CDRs themselves. More likely, despite the care taken in the design of the CDR-graft, the structural difference between the muV$_H$1 framework of 4G7 and the huV$_H$3 framework serving as acceptor framework led to some strain between CDRs and framework that limits the stability of the graft. Nonetheless, the stability of the loop donor was maintained.

The knowledge-based redesign with the individual amino acid substitutions was, therefore, capable of producing a variant of greater stability, and based on the biophysical properties, 4G7-mut is thus a candidate for the development of further derivatives intended for clinical use. However, the final choice will need to take into account the issue of immunogenicity, although for the therapy of human B-cell malignancies immunogenicity is not as severe a problem as for the treatment of solid tumors such as carcinomas, and the scientific basis of a lower immunogenicity of humanized molecules has been questioned (Clark, 2000). Additionally, the use as a fusion protein with e.g. protein toxins of plant or bacterial origin, may lower the importance of the immunogenicity of the scFv portion.

The final choice of the variant to be promoted further will thus depend on the exact therapeutic format chosen. The results of this study underscore the powers of the knowledge-based approach, but also illustrate some remaining difficulties in correctly predicting strain when bringing pieces from different proteins together.

Acknowledgements

The authors thank Prof. R. Levy from Stanford University for making the 4G7 hybridoma available, and PD Dr R. Slany for size exclusion chromatography. C.S. was the recipient of a stipend from the Bavarian Government (Bayerische Universitäten e.V.), and M.S. of a stipend from the Kind Phillip Foundation for leukemia research. We thank Hugues Bedouelle for providing the Kaleidagraph macros used to evaluate the equilibrium unfolding data.

Funding

This study was supported by grants from the W. Sander Foundation (No. 03.015.2), Deutsche Krebshilfe e.V. (No. 108242), the association 'Kaminkehrer helfen krebskranken Kindern e.V.', the Beitlich Foundation, Tübingen and the association of supporters of the University of Erlangen Children's Hospital (to G.H.F.). Part of this work was funded by an intramural grant from the ELAN fond and the Training Grant GK592 from the German Research Community (DFG).

References

Bargou,R., *et al*. (2008) *Science*, **321**, 974–977.
Benedict,C.A., MacKrell,A.J. and Anderson,W.F. (1997) *J. Immunol. Methods*, **201**, 223–231.
Bruenke,J., *et al*. (2004) *Br. J. Haematol.*, **125**, 167–179.
Bruenke,J., *et al*. (2005) *Br. J. Haematol.*, **130**, 218–228.
Carter,P., Bedouelle,H. and Winter,G. (1985) *Nucleic Acids Res.*, **13**, 4431–4443.
Chari,R.V. (2008) *Acc. Chem. Res.*, **41**, 98–107.
Clark,M. (2000) *Immunol. Today*, **21**, 397–402.
Eigenbrot,C., Randal,M., Presta,L., Carter,P. and Kossiakoff,A.A. (1993) *J. Mol. Biol.*, **229**, 969–995.
Erickson,H.K., Park,P.U., Widdison,W.C., Kovtun,Y.V., Garrett,L.M., Hoffman,K., Lutz,R.J., Goldmacher,V.S. and Blattler,W.A. (2006) *Cancer Res.*, **66**, 4426–4433.
Ewert,S., Honegger,A. and Plückthun,A. (2003a) *Biochemistry*, **42**, 1517–1528.
Ewert,S., Huber,T., Honegger,A. and Plückthun,A. (2003b) *J. Mol. Biol.*, **325**, 531–553.
Flavell,D.J., Warnes,S.L., Bryson,C.J., Field,S.A., Noss,A.L., Packham,G. and Flavell,S.U. (2006) *Br. J. Haematol.*, **134**, 157–170.
Greil,J., Gramatzki,M., Burger,R., Marschalek,R., Peltner,M., Trautmann,U., Hansen-Hagge,T.E., Bartram,C.R., Fey,G.H. and Stehr,K. (1994) *Br. J. Haematol.*, **86**, 275–283.
Grossbard,M.L., Press,O.W., Appelbaum,F.R., Bernstein,I.D. and Nadler,L.M. (1992) *Blood*, **80**, 863–878.
Hekman,A., Honselaar,A., Vuist,W.M., Sein,J.J., Rodenhuis,S., ten Bokkel Huinink,W.W., Somers,R., Rumke,P. and Melief,C.J. (1991) *Cancer Immunol. Immunother.*, **32**, 364–372.

Honegger,A. (2008) In Chernajovsky,Y.(eds.), *Therapeutic Antibodies*. Vol. 181. Springer-Verlag, Berlin-Heidelberg, pp. 47–68.
Honegger,A. and Plückthun,A. (2001a) *J. Mol. Biol.*, **309**, 657–670.
Honegger,A. and Plückthun,A. (2001b) *J. Mol. Biol.*, **309**, 687–699.
Honegger,A., Malebranche,A.D., Röthlisberger,D. and Plückthun,A. (2009) *Protein Eng. Des. Sel.*, (in press).
Hoogenboom,H.R. (2005) *Nat. Biotechnol.*, **23**, 1105–1116.
Jäger,M., Gehrig,P. and Plückthun,A. (2001) *J. Mol. Biol.*, **305**, 1111–1129.
Jung,S., Honegger,A. and Plückthun,A. (1999) *J. Mol. Biol.*, **294**, 163–180.
Jung,S., Spinelli,S., Schimmele,B., Honegger,A., Pugliese,L., Cambillau,C. and Plückthun,A. (2001) *J. Mol. Biol.*, **309**, 701–716.
Kabat,E.A., Wu,T.T., Perry,H., Gottesmann,K. and Foeller,C. (1991) *Sequences of Proteins of Immunological Interest*. Fifth edition, ed. NIH Publication No. 91-3242.
Kellner,C., *et al*. (2008) *J. Immunother*., **31**, 871–884.
Kipriyanov,S.M., Cochlovius,B., Schafer,H.J., Moldenhauer,G., Bahre,A., Le Gall,F., Knackmuss,S. and Little,M. (2002) *J. Immunol.*, **169**, 137–144.
Knappik,A., Ge,L., Honegger,A., Pack,P., Fischer,M., Wellnhofer,G., Hoess,A., Wölle,J., Plückthun,A. and Virnekäs,B. (2000) *J. Mol. Biol.*, **296**, 57–86.
Krebber,A., Bornhauser,S., Burmester,J., Honegger,A., Willuda,J., Bosshard,H.R. and Plückthun,A. (1997) *J. Immunol. Methods*, **201**, 35–55.
Lang,P., Barbin,K., Feuchtinger,T., Greil,J., Peipp,M., Zunino,S.J., Pfeiffer,M., Handgretinger,R., Niethammer,D. and Fey,G.H. (2004) *Blood*, **103**, 3982–3985.
Lefranc,M.P., Giudicelli,V., Kaas,Q., Duprat,E., Jabado-Michaloud,J., Scaviner,D., Ginestoux,C., Clement,O., Chaume,D. and Lefranc,G. (2005) *Nucleic Acids Res.*, **33**, D593–D597.
Lindner,P., Bauer,K., Krebber,A., Nieba,L., Kremmer,E., Krebber,C., Honegger,A., Klinger,B., Mocikat,R. and Plückthun,A. (1997) *BioTechniques*, **22**, 140–149.
Lonberg,N. (2005) *Nat. Biotechnol.*, **23**, 1117–1125.
Meeker,T.C., Miller,R.A., Link,M.P., Bindl,J., Warnke,R. and Levy,R. (1984) *Hybridoma*, **3**, 305–320.
Messmann,R.A., *et al*. (2000) *Clin. Cancer Res.*, **6**, 1302–1313.
Mirick,G.R., Bradt,B.M., Denardo,S.J. and Denardo,G.L. (2004) *Q. J. Nucl. Med. Mol. Imaging*, **48**, 251–257.
Monsellier,E. and Bedouelle,H. (2005) *Protein Eng. Des. Sel.*, **18**, 445–456.
Myers,J.K., Pace,C.N. and Scholtz,J.M. (1995) *Protein Sci.*, **4**, 2138–2148.
Nadler,L.M., Anderson,K.C., Marti,G., Bates,M., Park,E., Daley,J.F. and Schlossman,S.F. (1983) *J. Immunol.*, **131**, 244–250.
Nieba,L., Honegger,A., Krebber,C. and Plückthun,A. (1997) *Protein Eng.*, **10**, 435–444.
Ohage,E.C., Graml,W., Walter,M.M., Steinbacher,S. and Steipe,B. (1997) *Protein Sci.*, **6**, 233–241.
Olejniczak,S.H., Stewart,C.C., Donohue,K. and Czuczman,M.S. (2006) *Immunol. Invest.*, **35**, 93–114.
Pastan,I., Hassan,R., FitzGerald,D.J. and Kreitman,R.J. (2007) *Annu. Rev. Med.*, **58**, 221–237.
Peipp,M. and Valerius,T. (2002) *Biochem. Soc. Trans.*, **30**, 507–511.
Peipp,M., Saul,D., Barbin,K., Bruenke,J., Zunino,S.J., Niederweis,M. and Fey,G.H. (2004) *J. Immunol. Methods*, **285**, 265–280.
Pietersz,G.A., Wenjun,L., Sutton,V.R., Burgess,J., McKenzie,I.F., Zola,H. and Trapani,J.A. (1995) *Cancer Immunol. Immunother.*, **41**, 53–60.
Piscitelli,C.L., Angel,T.E., Bailey,B.W., Hargrave,P., Dratz,E.A. and Lawrence,C.M. (2006) *J. Biol. Chem.*, **281**, 6813–6825.
Press,O.W., Farr,A.G., Borroz,K.I., Anderson,S.K. and Martin,P.J. (1989) *Cancer Res.*, **49**, 4906–4912.
Proba,K., Honegger,A. and Plückthun,A. (1997) *J. Mol. Biol.*, **265**, 161–172.
Proba,K., Wörn,A., Honegger,A. and Plückthun,A. (1998) *J. Mol. Biol.*, **275**, 245–253.
Raffen,R., Dieckman,L.J., Szpunar,M., Wunschl,C., Pokkuluri,P.R., Dave,P., Wilkins Stevens,P., Cai,X., Schiffer,M. and Stevens,F.J. (1999) *Protein Sci.*, **8**, 509–517.
Röthlisberger,D., Honegger,A. and Plückthun,A. (2005) *J. Mol. Biol.*, **347**, 773–789.
Ruzheinikov,S.N., *et al*. (2003) *J. Mol. Biol.*, **332**, 423–435.
Santoro,M.M. and Bolen,D.W. (1988) *Biochemistry*, **27**, 8063–8068.
Sato,S., Miller,A.S., Howard,M.C. and Tedder,T.F. (1997) *J. Immunol.*, **159**, 3278–3287.
Schable,K.F., *et al*. (1999) *Eur. J. Immunol.*, **29**, 2082–2086.
Schindler,J., Sausville,E., Messmann,R., Uhr,J.W. and Vitetta,E.S. (2001) *Clin. Cancer Res.*, **7**, 255–258.
Schuermann,J.P., Henzl,M.T., Deutscher,S.L. and Tanner,J.J. (2004) *Proteins*, **57**, 269–278.
Schwemmlein,M., *et al*. (2007) *Leukemia*, **21**, 1405–1412.
Spada,S., Honegger,A. and Plückthun,A. (1998) *J. Mol. Biol.*, **283**, 395–407.
Stevens,F.J., Pokkuluri,P.R. and Schiffer,M. (2000) *Biochemistry*, **39**, 15291–11526.
Stieglmaier,J., *et al*. (2008) *Cancer Immunol. Immunother.*, **57**, 233–246.
Vallera,D.A., Todhunter,D.A., Kuroki,D.W., Shu,Y., Sicheneder,A. and Chen,H. (2005) *Clin. Cancer Res.*, **11**, 3879–3888.
van den Elsen,J., Vandeputte-Rutten,L., Kroon,J. and Gros,P. (1999) *J. Biol. Chem.*, **274**, 1495–1501.
Willuda,J., Honegger,A., Waibel,R., Schubiger,P.A., Stahel,R., Zangemeister-Wittke,U. and Plückthun,A. (1999) *Cancer Res.*, **59**, 5758–5767.
Wirtz,P. and Steipe,B. (1999) *Protein Sci.*, **8**, 2245–2250.
Wörn,A. and Plückthun,A. (1998) *Biochemistry*, **37**, 13120–13127.
Wörn,A., Auf der Maur,A., Escher,D., Honegger,A., Barberis,A. and Plückthun,A. (2000) *J. Biol. Chem.*, **275**, 2795–2803.
Wülfing,C., Lombardero,J. and Plückthun,A. (1994) *J. Biol. Chem.*, **269**, 2895–2901.
Yazawa,N., Hamaguchi,Y., Poe,J.C. and Tedder,T.F. (2005) *Proc. Natl Acad. Sci. USA*, **102**, 15178–15183.

Received October 3, 2008; revised November 28, 2008; accepted November 30, 2008

Edited by Hugues Bedouelle